International Journal of Solids and Structures 241 (2022) 111514

Contents lists available at ScienceDirect

International Journal of Solids and Structures

journal homepage: www.elsevier.com/locate/ijsolstr

Effect of tool size on the cutting of aluminum film with micrometer-level thickness

Xuan Ye [a], Tao Wang [b], Xiaoming Liu [a,c,*], Yueguang Wei [d]

[a] LNM, Institute of Mechanics, Chinese Academy of Sciences, Beijing 100190, China
[b] State Key Laboratory Explosion Science and Technology, Beijing Institute of Technology, Beijing 100081, China
[c] School of Engineering Science, UCAS, Beijing 100049, China
[d] College of Engineering, Peking University, Beijing 100871, China

ARTICLE INFO

Keywords:
Ductile film
Cutting force model
Branched concertina tear
Curling flap
Critical tool size

ABSTRACT

Cutting aluminum films with micrometer-level thickness requires a full understanding of the mixed effect due to bending, buckling, and fracture. These three deformation patterns have a strong relationship with the tool size. In this study, we present experimental, numerical, and theoretical studies of the tool size effect on a fracture. Using the energy analysis during a cut, we first build up a cutting force model that takes both the tool size and film thickness into account. The proposed model differs from previous models that used the ratio of size to thickness as the only factor. Our results first show that tool size affects fracture morphology. Films cut with large tools fail in the form of sequenced concertina tears, while films cut with small tools fail in the form of curling flaps. Furthermore, the transition of the two failure modes is theoretically presented with the critical value being obtained by the cutting force model proposed. Additionally, we find that when predicting the cutting force of aluminum films with micrometer-level thickness, the effect of fracture energy cannot be neglected. Increasing film thickness will decrease the effect of fracture energy on cutting force.

1. Introduction

Thin films are widely used in electronic devices such as functional semiconductor devices (Park et al., 2012; Nie and Kumacheva, 2008), sensors (Yokota, 2015; Zheng et al., 2016), and capacitors (Pan, 2018; Li, 2019), as well as in electronic packaging (Su et al., 2006; van den Broek et al., 2015; Cazón et al., 2017). To obtain devices of a certain size, cutting the fitted pieces with the help of fracture theory is a common method. Because of bending and buckling, the fracture of thin films is significantly different from the fracture of bulk materials. When a thin film is cut with a cylindrical tool, the pattern may vary depending on the ductility of the film and the size of the tool (Hamm et al., 2020; Ghatak and Mahadevan, 2003; Audoly et al., 2005).

For the cutting of a brittle thin film (Ghatak and Mahadevan, 2003; Roman, 2013; Roman et al., 2003), previous studies have shown that the oscillation of the crack path is attributable to the instability that occurs at the crack tip, which is controlled by the ratio of tool size to film thickness. This effect of tool size has been demonstrated by both experimental and numerical studies (Ghatak and Mahadevan, 2003; Audoly et al., 2005). When the tool diameter is smaller than the thickness, the stress profile is assumed to be a plane stress state for which the maximum hoop stress occurs ahead of the tool. As a result, the thin film is torn at the front of the tool so that a straight crack follows the trajectory of the tool. However, when the diameter of the tool is much bigger than the thickness, the interplay of the in-plane stretching and out-of-plane bending leads to an oscillatory fracture (i.e., going from a tensile fracture to a bending fracture). As a result, a path for this type of crack forms a regular tooth shape. This oscillatory fracture pattern has been confirmed by a numerical model (Audoly et al., 2005), which has demonstrated the geometrical origin. Overall, these studies share a common view that the crack path on brittle film will become straight when the size of the tool is reduced to the thickness of the film. In addition, some other studies have shown that the crack path is independent of cutting speed (Ghatak and Mahadevan, 2003; Reis et al., 2008) and boundary conditions. Additionally, tooth amplitude and wavelength have been found to be proportional to tool width (Ghatak and Mahadevan, 2003).

For the cutting of a ductile thin film, previous studies have suggested that the cutting mode changes with the tool sharpness (Zheng and Wierzbicki, 1996; Wierzbicki, 1995; Wierzbicki et al., 1998; Jin and Altenhof, 2011). The definition of sharpness—that is, whether a tool is

* Corresponding author at: LNM, Institute of Mechanics, Chinese Academy of Sciences, Beijing 100190, China.
E-mail address: xiaomingliu@imech.ac.cn (X. Liu).

https://doi.org/10.1016/j.ijsolstr.2022.111514
Received 4 September 2021; Received in revised form 7 February 2022; Accepted 13 February 2022
Available online 17 February 2022

Nomenclature

List of symbols

v	Cutting velocity
t	Film thickness
D	Cutting tool diameter
D/t	Ratio of tool size to film thickness
$(D/t)_{\mathrm{cr}}$	Critical ratio of tool size to film thickness
L_{tongue}	Tongue length
β	Deviation angle
R	Rolling radius
F_{curl}	Force required to form the curling flap
$\dot{E}_{bending}$	Energy dissipation rate of film bending
$\dot{E}_{membrane1}$	Rate of membrane energy in the near-tip zone
$\dot{E}_{membrane2}$	Rate of membrane energy in the tension–compression transition zone
$\dot{E}_{fracture}$	Rate of fracture energy
R_f	Specific work of fracture
θ	Wedge semi-angle
M_0	Fully plastic bending moment
σ_0	Flow stress
μ_s	Friction coefficient
λ	Wavelength of curling flap
λ_{exp}, λ_{theory}	Experimental and theoretical wavelengths
$\overline{F}_{indentation}$	Normalized axial indentation force
F_{tongue}	Tearing force perpendicular to concertina folds
$\overline{b}$, $\overline{b}_0$, $\overline{b}_t$	Normalized tear width, initial tear width, and ultimate tear width
$\overline{x}$	Normalized coordinate along the symmetry line
$(\overline{F}_{indentation})_{ave}$	Average tear force
$(\overline{F}_{indentation})_{min}$	Minimum value of force required for a concertina tear to occur

blunt or sharp—is similar to the study of brittle films (Ghatak and Mahadevan, 2003; Audoly et al., 2005), and the definition refers to the ratio of the shoulder width or tool diameter over the film thickness. When a tool is blunt, the cutting failure mode is concertina tearing (see Fig. 6), in which the film folds plastically and piles up ahead of the tool (Vandenberghe and Villermaux, 2013). Two diverging cracks are developed as the "concertina", which is named after the collapse pattern of circular tubes (Abramowicz and Jones, 1984; Guillow et al., 2001; Linul and Khezrzadeh, 2021). To clarify parallel concertina tearing, Wierzbicki et al. (Wierzbicki, 1995) assumed that at any instant the power input by the cutting force was related to the energy dissipation rate into plate bending, plate stretching, plate shearing, and plate fracture/tearing. Based on this assumption, they proposed a simplified model to predict the quasi-static cutting force on mild steel sheets (0.75–1.143 mm thick). Furthermore, they (Wierzbicki et al., 1998) developed the diverging concertina tearing theory and verified the theory with experiments on 0.4 mm-thick mild steel sheets. However, the tool geometries (e.g., shape and size) were not considered in these models.

When a sharp tool (wedge) cuts a ductile thin film, the failure mode becomes either braided (unstable) curling or clean (stable) curling (Magliaro and Altenhof, 2020) (see Fig. 6). The similarity between these two failure modes is that the fracture appears ahead of the tool. The difference is that for the former, the film is bent in an alternating manner, while for the latter, the film uniformly buckles and curls into flaps on each side of the tool. Zheng and Wierzbicki (Zheng and Wierzbicki, 1996) first assumed that a bent flap was composed of two cylindrical surfaces connected by a toroidal transition zone. Then, they postulated a curling flap model which showed that the cutting process had three different mechanisms of energy absorption. Imonsen and Wierzbicki (Simonsen and Wierzbicki, 1997) assumed two alternative deformation modes in the tip zone ahead of a cutting edge (i.e., the plastic flow mode and the crack-tip deformation mode) and proposed two curling flap theories for mild steel sheets with thicknesses in the range of 0.75–20.0 mm. However, these models did not consider fracture energy.

The three failure modes of ductile films mentioned above—concertina tearing, braided curling, and clean curling—are all steady-state responses. Before reaching a steady state, the pattern of cutting deformation has a transient feature (Zheng and Wierzbicki, 1996). The transient response usually causes a sheet to fracture at the wedge tip, which is characterized by the bending of the sheet along an inclined moving hinge. To understand the transient response process, Lu and Calladine (Lu and Calladine, 1990), Wierzbicki and Thomas (Wierzbicki and Thomas, 1993), Paik (Paik, 1994), and Ohtsubo and Wang (Ohtsubo and Wang, 1995) theoretically investigated mild or high-tensile steel sheets with millimeter-level thicknesses subjected to quasi-static wedge cutting. Additionally, Jones et al. (Jones and Jouri, 1987), Vaughan et al. (Vaughan, 1980), and Woisin (Woisin, 1982) investigated the dynamic effects of sheets subjected to the impact of a falling hammer. The assumptions, scope of application, and deficiencies of the above models are summarized in Table 1.

In general, previous experimental and theoretical studies have been conducted for ductile films or sheets with thicknesses at the millimeter level or above. However, there is a lack of systematic research on films with micrometer-level thicknesses. Specifically,

1) There is a lack of cutting experiments for ductile films with tools of different diameters.
2) For the concertina tearing model, the effect of tool shape and size on the cutting force has not been considered.
3) For the curling flap model, the contribution of fracture energy to cutting force has not been considered. As we find in our experiment, this effect cannot be ignored when the film is ultrathin.

In this study, we focus on the steady-state cutting of a ductile thin film. As can be seen in the experiments shown in Fig. 1, the branching of the tearing fracture appears rather than the typical concertina in previous studies of ductile film (Zheng and Wierzbicki, 1996; Wierzbicki, 1995). The reason for the bifurcation of the fracture has not been studied. Furthermore, previous studies considered that the sheet fracture pattern only depended on the ratio of tool size to sheet thickness, as in studies of a tool with a wedge (Zheng and Wierzbicki, 1996). However, by analyzing the energy contributions of stretching, bending, and fracture during the cut, we find that the above conclusion is suitable for thick films and not for thin films. This is because both fracture and stretching energies scale like sheet thickness t, while the bending energy (Audoly and Pomeau, 2010) scales like t^4. Therefore, the dominant energy term should switch from bending energy to fracture or stretching energy as the film becomes thinner. This switch will depend not only on the ratio of tool diameter to film thickness but also on film thickness.

To investigate how the fracture pattern switches during the cutting of thin aluminum films, we first perform experimental and numerical studies and then develop a new cutting force model with energy analysis. By comparing the energy contributions during cutting, we build up a force model that takes both tool size and film thickness into account. The proposed model differs from previous models, which used the ratio of tool size to thickness as the sole factor. By using this new model, we

Table 1
Assumptions and application scope of various cutting models.

Cutting tool	Exp method	Material	t (mm)	Failure modes	Model/Assumptions	Cutting force	Remarks	Ref.
Round-nosed wedge $r=15$ mm, $2\theta=60^\circ$	–	–	–	Transient (or initial) wedge penetration	Based on an empirical formula proposed for ship collision problems.	F=(33900 t + 190tltanθ)/cosα	–	Vaughan (Vaughan, 1978)
Wedge, $\theta=5^\circ$,15°, 30°, $\alpha=10^\circ$	Drop-hammer tests	Unstiffened mild steel plate	0.75–1.9	–	Assumption: Energy is absorbed in two ways: plastic deformation and the creation of new surfaces with a fracture.	F=(5500 $t^{1.5}$ + 8.8lt^2tanθ)/cosα	For small penetrations, the formulas did not correspond to actual forces.	Vaughan (Vaughan, 1980)
Wedge, $\theta=15^\circ$,35°,50°, $\alpha=0^\circ$	Drop-hammer tests	Mild steel plate	2–4	–	Assumption: energy absorption.	$F=2500\,t^2[0.5+(0.05+0.004\,l/t)(\theta$-20°)/15°] for $20^\circ\le\theta\le50^\circ$ and $24\le l/t\le60$	–	Woisin (Woisin, 1982)
Wedge, $2\theta=15^\circ$,30°,45°,60°, $\alpha=0^\circ$	Drop-hammer tests	Unstiffened mild/high-tensile steel plate	1.501–5.95	–	Assumptions: Energy-absorbing mechanisms-cutting, curling, or distorting, elastic, and frictional energy. The bending and friction energies were found to amount to about 10% each, and the elasticity effect was ignored.	(1) $F=3900\,t^{1.44}$ for $t=1.501$ mm, $\sigma_0=255$ MPa (2) $F=7200\,t^{1.305}$ for $t=3.25$–5.95 mm, $\sigma_0=398.5$ MPa	For the plate cutting problem, the geometrically similar scaling principle was not satisfied.	Jones (Jones and Jouri, 1987)
Wedge, $2\theta=20^\circ$,40°, $\alpha=0^\circ$	Quasi-static cutting tests	Unstiffened high-tensile steel plate	0.72–2.0	Transient (or initial) wedge penetration	A simple empirical formula based on Buckingham's dimensional analysis. Assumption: The yield stress is the only relevant material property.	$F=1.3C_{1.3}\sigma_0 l^{0.3}t^{1.7}$ for $5<l/t<150$	$C_{1.3}$ is a purely empirical constant depending on cutting conditions.	Lu (Lu and Calladine, 1990)
Wedge, $10^\circ\le\theta\le30^\circ$	Quasi-static cutting tests	–	–	Transient (or initial) wedge penetration	An approximate kinematic model combines the effects of plasticity, fracture, and friction into a single-term formulation. Assumption: The plate material curls up into two inclined cylinders when the wedge advances into the plate.	$F=3.28\sigma_0\mu^{0.4}l^{0.4}t^{1.6}\delta_t^{0.6}$for $0.1\le\mu\le0.4$	–	Wierzbicki (Wierzbicki and Thomas, 1993)
Wedge, $2\theta=15^\circ$,30°,45°,60°, $\alpha=0^\circ$	Quasi-static cutting tests	Longitudinally stiffened steel plate	3.4–7.8	Transient (or initial) wedge penetration	Based on dimensional analysis. Assumptions: (1) Longitudinal stiffeners are included by using an area equivalent plate thickness t_{eq} (2) The inertia effect is negligible.	$F=1.5C_{1.5}C_f\sigma_0 t_{eq}{}^{1.5}l^{0.5}/\cos\alpha$, where the coefficient $C_{1.5}=1.112$–$1.156\theta+3.76\theta^2$, the dynamic correction factor $C_f=1.0$–$0.042v+0.001v^2$, and the initial impact velocity v	$C_{1.5}$ might change for different materials or test conditions.	Paik (Paik, 1994)
Wedge	Quasi-static cutting tests	–	–	Steady-state (with the stable flap buckled)	A kinematic model with only one free parameter, the plate rolling radius R. Assumptions: (1) A bent flap is composed of two cylindrical surfaces connected by a toroidal transition zone (2) Energy-absorbing mechanisms: a) plate bending in moving hinge lines, b) membrane deformation (near the wedge tip and tension–compression transition zone).	$F=2Bt\sigma_0(1+\mu_s\cot\theta)[2(B+R)/R+1.46R\cos\theta/t+1.28\theta^2(B+R)^2\cos(0.5\theta)/Rt]$, where the rolling radius $R=[(2\,t/B+1.28\theta^2\cos(0.5\theta))/(1.46\cos\theta+1.28\theta^2\cos(0.5\theta))]^{0.5}$	The fracture effect was not considered.	Zheng (Zheng and Wierzbicki, 1996)
Wedge	Quasi-static cutting tests	–	–	Transient (or initial) wedge penetration	A kinematic model is proposed. Assumptions: (1) No separation between the wedge tip and crack tip. (2) The plate material separates ahead of the wedge tip and then curves into two surfaces of variable curvature. (3) Energy-absorbing mechanisms: membrane plastic flow in the near-tip field and bending of the plastic hinges.	$F=1.51\sigma_0 t^{1.5}l^{0.5}(\sin\theta)^{0.5}(1+\mu/\tan\theta)$	–	Ohtsubo (Ohtsubo and Wang, 1995)
Wedge		Mild steel plate	0.75–1.143			$F=4.33\sigma_0 t^{5/3}b^{1/3}+8/3Rt$		

(*continued on next page*)

Table 1 (*continued*)

Cutting tool	Exp method	Material	t (mm)	Failure modes	Model/Assumptions	Cutting force	Remarks	Ref.
	Quasi-static cutting tests			Parallel concertina tearing	Based on the concept of stationary tension/compression, shear and bending hinge lines with slope discontinuities and rigidly displacing and rotating plate elements. Assumption: Energy-absorbing mechanisms: plate bending, stretching (membrane action), shearing, and fracture/tearing.		The actual punch shape and size were not considered.	Wierzbicki (Wierzbicki, 1995)
Wedge, $\theta = 10^{\circ}$,30°,45°, $\alpha = 10^{\circ}$	Quasi-static cutting tests	Mild steel plate	0.75, 1.6, 20.0	Steady-state cutting	Assumptions: (1) Energy dissipation mechanisms: a plastic-tip zone, moving bending hinge lines, and a membrane deformation zone (2) The membrane deformation zone is dominated by plastic shear strains (3) Two alternative deformation modes in the tip zone in front of the cutting edge: a purely plastic flow mode and a plastic fracture mode.	(1) plastic flow mode: $F = g(\mu,\theta,\alpha)[0.64/3^{0.5}\sigma_0 tR(\cos\theta)^2(1+0.55\theta^2) +2*3^{-0.5}\sigma_0 tB\theta + \sigma_0 t^2/3^{0.5}(B+R)/R/\cos\theta]$, R=…, $R \le 1.75B$ (2) crack-tip deformation mode: $F = g(\mu,\theta,\alpha)[G_c t + 2*3^{-0.5}\sigma_0 tB\theta + 1.57\sigma_0 t^2/3^{0.5}/\cos\theta]$	The contribution of the tip zone in cutting and tearing was not clear. Dynamic effects were not included.	Simonsen (Simonsen and Wierzbicki, 1997)
Blunt/rounded wedge	Quasi-static cutting tests	Mild steel plate (with an initial precut width)	0.4	Diverging concertina tearing	Assumptions: (1) Energy dissipation mechanisms: uncoupled plate bending, plate membrane action, shear action, and plate fracture/tearing (2) The plate resistance is independent of the punch geometry and friction coefficient.	$F = M_0(9.35b^{1/3} + 0.56b^{2/3} + 4*3^{1/2}R/\sigma_0/t)$, where width $b = 0.32H^2 + 0.8H^{1.5}$	The actual punch shape and size were not considered.	Wierzbicki (Wierzbicki et al., 1998)

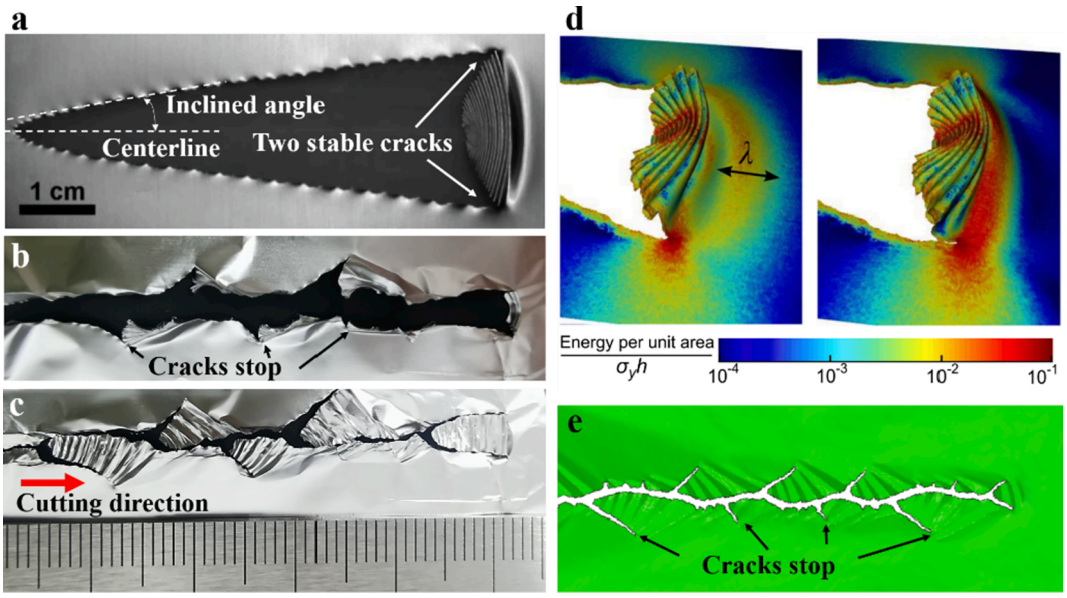

Fig. 1. Different types of fracture morphology. (a) A traditional type of concertina tearing found in the references (Wierzbicki, 1995; Tallinen and Mahadevan, 2011), where two stable cracks propagate, generating a folded tongue. Reproduced with permission (Tallinen and Mahadevan, 2011). Copyright 2011, American Physical Society. (b) Our experiments show periodic concertina tearing in 10 μm-thick aluminum film cut by a 5.22 mm cylindrical tool, where one crack of the tongue stops, forming the branch of the tear. (c) The same image as in (b) with the folds smoothed. (d) Simulations that reproduce the experimental concertina tearing shown in (a). The colors indicate the intensity of the elastic energy. Reproduced with permission (Tallinen and Mahadevan, 2011). Copyright 2011, American Physical Society. (e) Our simulation of the branched concertina tearing in (c).

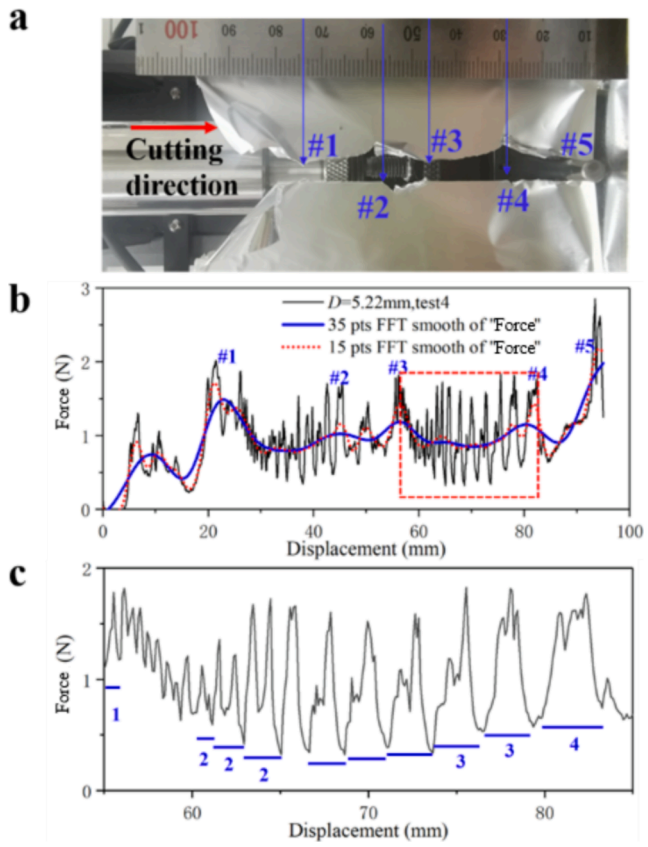

Fig. 2. (a) Branched tear and (b) force–displacement curve for a 5.22 mm cylindrical tool. #1-#5 represent the starting positions of each tongue. (c) Force-displacement curve for tongue #3 in Fig. 2a and 2b.

predict the cutting forces for the three film thicknesses, and we verify them with corresponding experiments.

2. Experimental results

In this study, we cut aluminum films (from 10 μm to 25 μm thick) with a tool at a constant velocity v. The tool is a cylinder with a diameter approximately 1 to 500 times the thickness. As shown in Fig. A1 in the Appendix, the film has a rectangular shape, with dimensions of 100 mm × 40 mm. The two long edges of the film are clamped on a U-shaped frame with double-sided tapes, and one short edge of the film is fabricated with an initial crack (5 mm) in the middle. The direction of the crack is parallel to the long edge, and during the experiments, the middle crack is extended by a cylindrical tool cutting in the vertical direction.

As we found in our experiment for ductile film, the branch of tearing appeared rather than the traditional concertina tearing from the previous studies (Tallinen and Mahadevan, 2011; Zheng and Wierzbicki, 1996; Wierzbicki, 1995). In previous studies, as shown in Fig. 1a, 1d, two stable cracks propagated during the cut, generating a folded tongue along the centerline. With a different crack pattern, our experiments (aluminum films with a 10 μm thickness cut by a 5.22 mm cylindrical tool) show concertina tearing with periodic branches (Fig. 1b). In this case, one crack of the tongue stops, forming the branch of the tear. For better observation, we smooth the tongues of the branched concertina shown in Fig. 1b. The smoothed structure is shown in Fig. 1c. This pattern indicates that the wavelength of the folding increases during the formation of each tongue. In addition, the force–displacement curve during this branched tear is recorded, with the peak force indicating the initial tear of each new concertina (marked with blue numbers in Fig. 2a, b). Additionally, we observe the force variation for a single concertina, e.g., tongue #3 in Fig. 2a. In this case, the force–displacement curve shows that a complete fold is formed at the beginning of the cut, and two small folds converge into a single fold as the displacement increases; at a later stage of the cut, three or even four small folds converge into a single fold (Fig. 2c).

During a single cut with other tool sizes, as shown in Fig. A2 of the

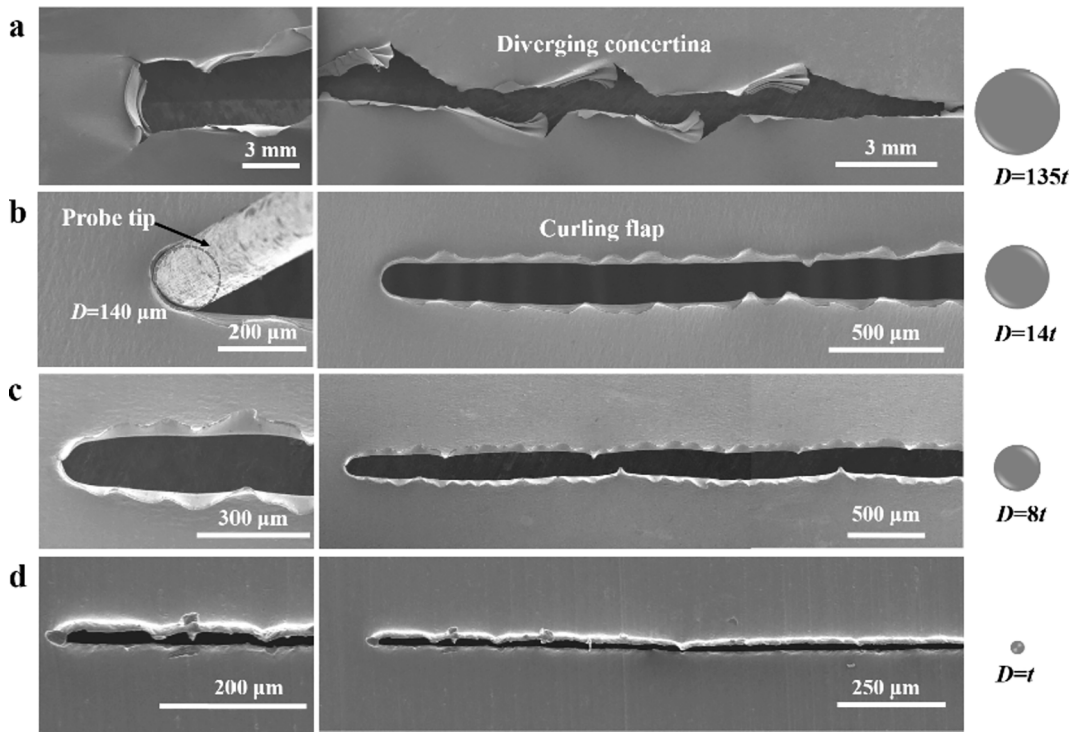

Fig. 3. Tool size-dependent morphologies of cracks in 10 μm-thick aluminum film with in-situ experiments in the SEM and atmospheric environments. (a) Tool diameter $D = 135\,t$. (b) $D = 14\,t$. (c) $D = 8\,t$. (d) $D = t$. When the ductile film is cut with large cylindrical tools (with large D/t), the film fails with multiple concertina tears. When the film is cut with small tools (with small D/t), the film fails with curling flaps.

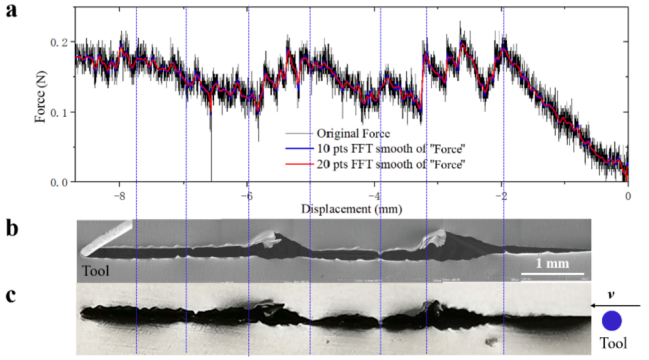

Fig. 4. In-situ cutting experiments of thin films performed with a 140 μm-diameter cylindrical tool. (a) Load-displacement curve. (b) SEM image and (c) Optical image.

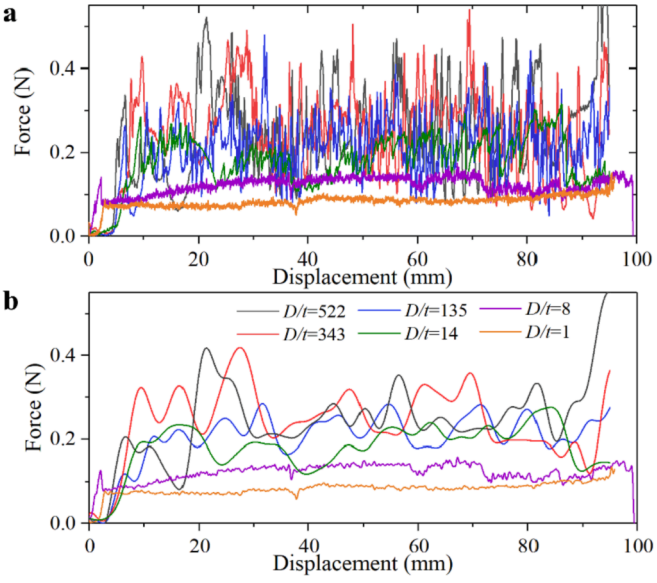

Fig. 5. Typical force–displacement curves for cutting 10 μm-thick film using tools of different sizes. (a) Original and (b) averaged force–displacement curves.

Appendix, we smooth the tongues and measure their lengths. The result shows a linear relationship between the tongue length and the tool diameter. Moreover, we carry out a numerical analysis by finite element method (FEM) that combines the finite elastic–plastic deformation with the damage to reproduce the observed fracture morphologies in the experiment. Simulation details can be found in Appendix A. By taking the same input parameters as those in the experiment, the finite element simulation (Fig. 1e) reproduces similar results to the experimental concertina tearing shown in Fig. 1c.

Unlike the concertina tearing that occurs when the film is cut with a large cylindrical tool ($D/t = 135$, Fig. 3a), a periodic stick–slip phenomenon is observed in experiments with very small tools (D/t less than 8; see the movie in the Support Information). During the cut with small tools, the film fails with a central crack and forms curling flaps on both sides of the crack (Fig. 3c-d). However, the in-situ experiment shows that both concertina tearing and a periodic stick–slip phenomenon can appear when $D/t = 14$, as shown in Fig. 4 (Fig. 3b is part of Fig. 4). This fact confirms that the critical D/t corresponding to the transition when the failure mode occurs is around 14. Another piece of evidence is the force history. When the tool size is smaller than the critical size, both the average and the fluctuation of the cutting force decrease rapidly (Fig. 5).

For a traditional concertina tear (Fig. 1a), as the tool advances, two steady-state cracks propagate with inclined angles; as a result, the tongue length and the cutting force also increase (Wierzbicki et al., 1998). By contrast, in our experiment, we observe a sequence of branched concertina tears during the cut (Fig. 2a and Fig. A2). The width

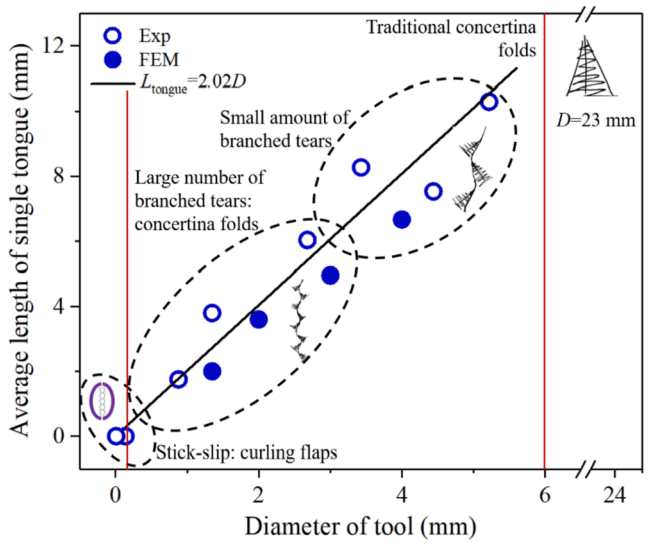

Fig. 6. Linear dependence of tongue length and tool size, shown by the blue circles. The inset shows the size-dependent fracture pattern on the film (film thickness is 10 μm). (For interpretation of the references to colour in this figure legend, the reader is referred to the web version of this article.)

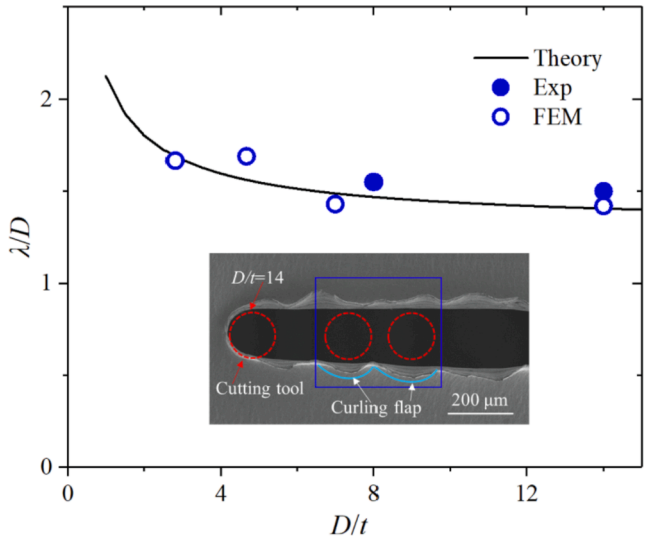

Fig. 7. Comparison of theoretical predictions, experimental measurements, and numerical simulations of the normalized curling flap wavelength with different tool diameters. The inset is an example of $D/t = 14$ ($D = 140$ μm, $t = 10$ μm), and the experimentally measured curling flap wavelength is $\lambda_{exp} = 215$ μm (~1.5D), which is close to the theoretical wavelength $\lambda_{theory} = 1.41D$.

of the tongue is limited by the tool diameter. Furthermore, the length of the tongue does not increase indefinitely with the increasing displacement of the cutting tool. In a different way, the tongue stops stacking at a distance where the next concertina tear initiates (Fig. A3). This is caused by the instability of the crack propagation during concertina tearing. Taking tongues #1 and #2 as examples, when the width of tongue #1 reaches half of the tool diameter ($W_{\text{tongue}} = D/2$), tongue #1 stops, and tongue #2 initiates (Fig. A3). Assuming that the outer contour of the tongue is triangular, the theoretical length of the tongue can be obtained as $L_{\text{tongue}} = D/2/\sin\beta$ according to the geometric relationship, where β is the deviation angle. Through the image processing of the results shown in Fig. A2, it can be determined that the deviation angle is in the range of $\beta \in (11^{\circ}, 15^{\circ})$. Therefore, the theoretical L_{tongue} is between 1.93D and 2.62D. Specifically, for the traditional cutting of ductile films

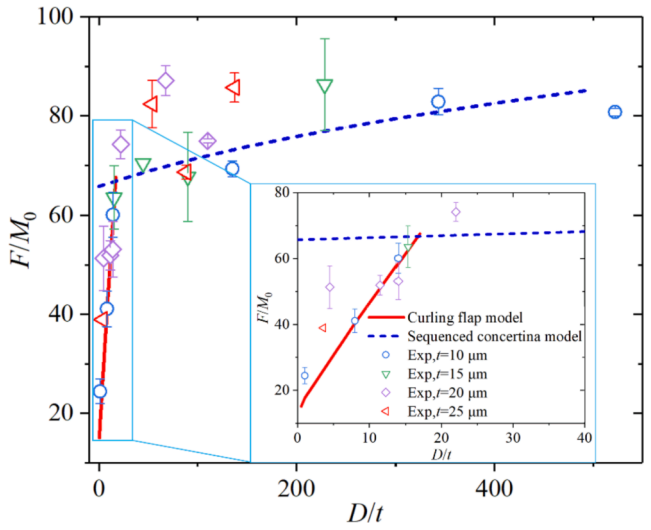

Fig. 8. Comparison of theoretical predictions and experimental results for the cutting forces required for aluminum films with thicknesses of 10–25 μm with different tool diameters. There is a critical $(D/t)_{cr} \sim 15$. When $D/t < (D/t)_{cr}$, the failure mode is a curling flap; when $D/t \geq (D/t)_{cr}$, the failure mode is sequenced concertina tearing. Inset: enlarged view of the relationship between the cutting force and the tool diameter. The error bars represent the standard deviation.

(Wierzbicki et al., 1998), since the prefabricated crack width is greater than the tool size (diameter), two cracks can only propagate continuously forward along the fixed angle and finally form a symmetrical tongue.

Through image processing for the results shown in Fig. A2, the experimental average tongue length (shown by the hollow circles in Fig. 6) can also be obtained. For a deeper understanding of the failure mode, we draw a schematic diagram of the average tongue length L_{tongue} and the failure mode for tools with different diameters (Fig. 6). The experimental results show a linear relationship between L_{tongue} and the tool diameter D, which can be fitted as

$$L_{tongue} = 2.02D \tag{1}$$

Furthermore, the tongue length can be obtained with numerical simulation, as shown by the solid circles in Fig. 6. We compare the theoretical and numerical predictions and the experimental measurements of the average tongue lengths, and we find that the theoretical results agree well with the experimental and FEM results.

3. Theoretical model for cutting force

Figs. 3 and 6 show that the fracture pattern of micron-thickness film depends on the tool size. When cut with a sharp tool, the film fails mainly with curling flaps; when cut with a blunt tool, the film breaks with branched concertina tears. As an extreme case, when the tool is very blunt, the film fails with a traditional concertina tear ($\beta = 0$). This fact indicates that the failure of the film is different with the different tool sizes. Therefore, corresponding theoretical models are required for the specific failure modes. By analyzing the energy contribution of all components during the cut, we propose two force models: the curling flap model for small D/t is described in Section 3.1 and the branched concertina tearing model for large D/t is described in Section 3.2. Furthermore, we obtain the critical $(D/t)_{cr}$ corresponding to the transition of the two failure modes that are described in Section 3.3. In addition, we find that the self-similarity (Zheng and Wierzbicki, 1996) of the ratio is questionable when the film thickness is reduced to micron size; this discussion is in Section 3.4.

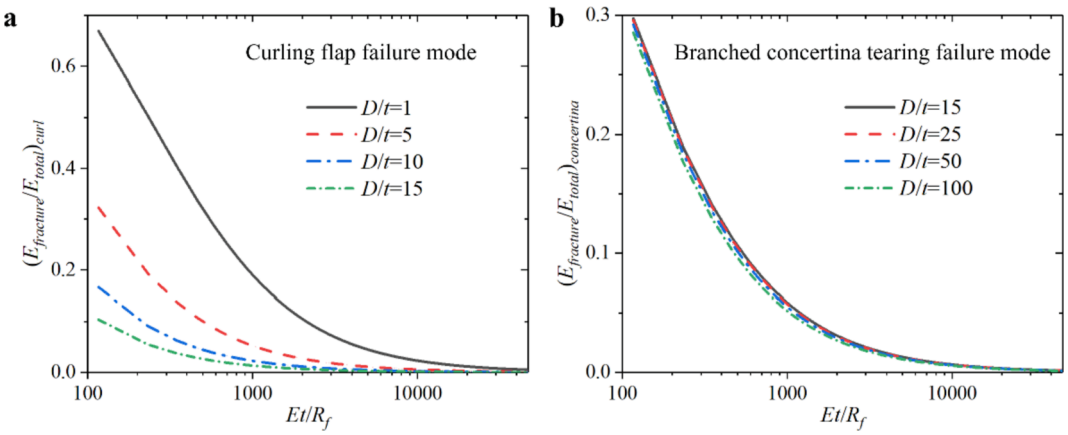

Fig. 9. Effect of fracture energy on cutting force in (a) curling flap and (b) sequenced concertina failure modes. For both failure modes, the effect of the fracture energy on the cutting force decreases with the increasing film thickness. When $Et/R_f > 20000$ the contribution of the fracture energy to the total energy is (a) less than 1.2% for the sharp tools and (b) less than 0.33% for the blunt tools. Additionally, for the sequenced concertina failure mode, the energy ratio is insensitive to D/t.

3.1. Curling flap model for small D/t

In the Appendix, Fig. A4 shows the morphology of the original curling flap formed after cutting the film with a sharp cylindrical tool (Fig. A4a) and after the smoothing treatment (Fig. A4b). From Fig. A4b, we find that the size and the period of the curling flap are related to the tool size (red circles in the enlarged view of Fig. A4b). As described in reference (Zheng and Wierzbicki, 1996), the periodic transition zone between each two curling flaps is caused by film deformation. The transient flap is first stretched to form the transition zone, and then compressed to form the stable curling flap. Also, the in-plane compression force causes the film to buckle near the ridge of stable curling flap. In addition, the FEM results also confirm the similar phenomenon of a curling flap near the cylindrical tool (Fig. A5). A curling flap model was proposed by Zheng et al. (Zheng and Wierzbicki, 1996) for cutting film using a wedge-shaped tool. Based on their model, we assume a loop of a plastic hinge at a distance R from the surface of the cylindrical tool (Fig. A5c). The difference is that our model includes the fracture energy, whereas previous study (Zheng and Wierzbicki, 1996) did not consider the effect of the fracture energy.

The fracture energy needs to be considered in this research. This is because both the fracture energy and the stretching energy scale like t, while the bending energy scales like t^4. Therefore, as the film becomes thinner, the dominant energy term should switch from bending to fracturing or stretching. The thin film in this research has a thickness of only 0.01 mm, while the films in the previous study (Zheng and Wierzbicki, 1996) had thicknesses in the range of 0.75 mm to 20 mm. Our later discussion in Section 3.4 shows that the fracture energy cannot be neglected for a film with a micro size thickness.

During the cutting, the external input work is assumed to be equal to the dissipation energy of the bending, membrane, and fracture

$$F_{curl}v = \dot{E}_{bending} + \dot{E}_{membrane1} + \dot{E}_{membrane2} + \dot{E}_{fracture} \tag{2}$$

where F_{curl} is the external force required to form the curling flap, $\dot{E}_{bending}$ is the energy dissipation rate of the film bending. $\dot{E}_{membrane1}$ and $\dot{E}_{membrane2}$ are the rates of the membrane energy in the near-tip zone and the tension–compression transition zone, respectively. The expressions of these three components of the energy dissipation rate are from the literature (Zheng and Wierzbicki, 1996) and listed in Appendix B. $\dot{E}_{fracture}$ is the rate of the fracture energy, which can be expressed as (Wierzbicki et al., 1998)

$$\dot{E}_{fracture} = R_f t v \tag{3}$$

where R_f is the specific work of the fracture at the crack tip, and the value of R_f is 3 N/mm for aluminum film. We assume that the cylindrical tool approximates a wedge-shaped tool with a wedge semi-angle $\theta = \pi/4$ and a wedge semi-width $D/2$, and we normalize the external force F_{curl} with the fully plastic bending moment (Zheng and Wierzbicki, 1996; Wierzbicki et al., 1998) M_0, defined by:

$$M_0 = \left(\frac{2}{\sqrt{3}}\sigma_0\right)\frac{t^2}{4} \tag{4}$$

where σ_0 is the flow stress. Then the dimensionless external force required to form the curling flap can be written as

$$\overline{F}_{curl} = \frac{F_{curl}}{M_0} = 2\frac{R+\frac{D}{2}}{R} + 1.268\frac{R}{t}cos\theta + 1.28\theta^2\frac{\left(R+\frac{D}{2}\right)^2}{Rt}\frac{cos\left(\frac{\theta}{2}\right)}{cos\theta} + 2\sqrt{3}\,\frac{R_f}{\sigma_0 t} \tag{5}$$

where R is the unknown rolling radius. Moreover, considering the friction effect between the cutting tool and the film, the normalized cutting force can be rewritten as

$$\overline{F}_{curl} = \left[2\frac{R+\frac{D}{2}}{R} + 1.268\frac{R}{t}cos\theta + 1.28\theta^2\frac{\left(R+\frac{D}{2}\right)^2}{Rt}\frac{cos\left(\frac{\theta}{2}\right)}{cos\theta} + 2\sqrt{3}\,\frac{R_f}{\sigma_0 t}\right]\cdot(1+\mu_s cot\theta) \tag{6}$$

where μ_s is the friction coefficient with a value of 0.2. The assumption that the rolling radius R is adjustable to minimize the normalized cutting force gives

$$\frac{\partial \overline{F}_{curl}}{\partial R} = 0 \tag{7}$$

After substituting Eq. (6) into Eq. (7), the solution of Eq. (7) is

$$\frac{R}{D} = 0.5\sqrt{\frac{4\left(\frac{t}{D}\right) + 1.28\theta^2 cos\left(\frac{\theta}{2}\right)}{1.268cos\theta + 1.28\theta^2 cos\left(\frac{\theta}{2}\right)}} \tag{8}$$

Additionally, by combining the theory with the schematic diagram in Fig. A5c, the normalized wavelength $\bar{\lambda}$ of the curling flap can be calculated as

$$\overline{\lambda} = \frac{\lambda}{D} = \frac{\frac{1}{4}\pi(D+2R)}{D} = \frac{1}{4}\pi\left(1+\sqrt{\frac{4\left(\frac{t}{D}\right)+1.28\theta^2 cos\left(\frac{\theta}{2}\right)}{1.268cos\theta+1.28\theta^2 cos\left(\frac{\theta}{2}\right)}}\right) \tag{9}$$

In summary, we provide a theoretical prediction of the wavelength of the curling flap in Eq. (9). Then, with two different tool diameters, we compare the theoretical predictions, experimental measurements, and numerical results of the normalized curling flap wavelength, and we find that the theoretical results agree well with the experimental and FEM results, as shown in Fig. 7. The inset is an example with $D/t = 14$. The measured wavelength of the curling flap is $\lambda_{exp} \sim 1.5D$, which is close to the theoretical wavelength $\lambda_{theory} = 1.41D$.

3.2. Branched concertina tearing model for large D/t

The traditional concertina tearing model proposed by Wierzbicki et al. (Wierzbicki et al., 1998) indicates that the cutting force is determined by the fracture toughness, flow stress, and thickness of a film and that the cutting force increases continuously with the increase of the cutting displacement. Furthermore, in their model, the cutting force or the concertina tearing length is independent of the tool size. Our experimental results show that there is a limit to the tongue length (Fig. 6), so the cutting force cannot increase infinitely with the increasing tool displacement. When the tongue length reaches the critical length (provided by Eq. (1)), the current tearing stops, and the next new concertina tearing starts (as shown in Fig. 1b and 1e).

In the sequenced concertinas, with the deviation angle β from the cutting direction (Fig. A3), the normalized axial indentation force (cutting force) can be expressed as

$$\overline{F}_{indentation} = \frac{F_{indentation}}{M_0} = \frac{\left(\frac{F_{tongue}}{cos\left(\frac{\beta}{2}\right)}\right)}{M_0} \tag{10}$$

where the tearing force perpendicular to the folds of a single concertina is defined as (Wierzbicki et al., 1998)

$$F_{tongue} = \left(9.35\overline{b}^{1/3} + 0.56\overline{b}^{2/3} + 4\sqrt{3}\ \frac{R_f}{\sigma_0 t}\right)M_0 \tag{11}$$

The normalized tear width $\overline{b}$ is denoted as

$$\overline{b} = \left(3x + \overline{b}_0^{4/3}\right)^{3/4} \tag{12}$$

where $\overline{x} = \frac{x}{t}$ is the normalized coordinate along the symmetry line originating from the tear start point, and $\overline{b}_0$ is the normalized initial tear width defined in reference (Wierzbicki et al., 1998). Here, the initial tear width equals to the prefabricated crack width in experiments. The starting point or starting criterion for each new concertina tear is

$$\overline{x} = 0 \tag{13}$$

At this beginning of a new concertina tear, the normalized tear width is: $\overline{b} = \overline{b}_0$. In consequence, the initial axial indentation force (cutting force) can be expressed as

$$\overline{F}_{indentation}|x=0 = \frac{\left(9.35\overline{b}_0^{1/3} + 0.56\overline{b}_0^{2/3} + 4\sqrt{3}\ \frac{R_f}{\sigma_0 t}\right)}{cos\left(\frac{\beta}{2}\right)} \tag{14}$$

By considering the critical tongue length in Eq. (1), the ending length $\overline{x}_t$ for this concertina tear can be derived as

$$\overline{x}_t = \frac{L_{tongue}cos\left(\frac{\beta}{2}\right)}{t} = 2.02D\frac{cos\left(\frac{\beta}{2}\right)}{t} \tag{15}$$

By substituting Eq. (15) into Eq. (12), the ultimate tear width can be obtained as $\overline{b}_t = \left(3\overline{x}_t + \overline{b}_0^{4/3}\right)^{3/4}$. Similarly, by substituting b_t into Eq. (10), the normalized axial indentation force at the ending point can be obtained as

$$\overline{F}_{indentation}|_{\overline{x}=\overline{x}_t} = \frac{\left(9.35\left(3x_t + \overline{b}_0^{4/3}\right)^{1/4} + 0.56\left(3x_t + \overline{b}_0^{4/3}\right)^{1/2} + 4\sqrt{3}\ \frac{R_f}{\sigma_0 t}\right)}{cos\left(\frac{\beta}{2}\right)} \tag{16}$$

Since the conventional concertina tearing model (Wierzbicki et al., 1998) shows that the cutting force varies approximately linearly with the tool displacement during concertina tearing, an average of the cutting force during the whole tearing process can be taken. The averaged cutting force can be expressed with

$$\left(\overline{F}_{indentation}\right)_{ave} = 0.5\left(\overline{F}_{indentation}|\overline{x}=0\ +\ \overline{F}_{indentation}|\overline{x}=\overline{x}_t\right) \tag{17}$$

The deviation angle is $\beta \in (11°, 15°)$, so the variation of $cos(\frac{\beta}{2})$ in the range is within 0.4%. As a result, $\beta = 11°$ can be taken for simplification.

We compare the theoretical predictions and the experimental results for the cutting forces required for aluminum films with thicknesses of 10 μm to 25 μm. As shown in Fig. 8, the results with the tool size D up to 500 t agree well with the theoretical predictions in Eq. (6) and Eq. (17). Additionally, Fig. 8 shows a critical transition at around $(D/t)_{cr} \sim 15$. When $D/t < (D/t)_{cr}$, the failure mode is a curling flap; when $D/t \geq (D/t)_{cr}$, the failure mode changes to sequenced concertina tearing.

3.3. Critical $(D/t)_{cr}$ corresponding to the transition of the failure mode

Fig. 8 shows that the fracture pattern of the film changes from a curling flap to branched concertina tearing as D/t increases. The transition of the failure mode can be obtained with

$$\left(\overline{F}_{curl}\right)_{ave} = \left(\overline{F}_{indentation}\right)_{min} \tag{18}$$

The right side of Eq. (18) is the normalized initial axial indentation force $\overline{F}_{indentation}|\overline{x}=0$, as shown in Eq. (14). With $\overline{D} = D/t$, $\overline{R} = R/t$, and $\alpha = \overline{R}/\overline{D}$, the normalized expression of Eq. (8) is

$$\alpha = \frac{\overline{R}}{\overline{D}} = 0.5\sqrt{\frac{4/\overline{D}+1.28\theta^2 cos(\theta/2)}{1.268cos\theta+1.28\theta^2 cos(\theta/2)}} \tag{19}$$

Then with $\mu_s = 0$, Eq. (18) can be reduced to

$$2+\frac{1}{\alpha}\ +\ 1.268\alpha\overline{D}cos\theta + 1.28\theta^2\frac{cos(\theta/2)}{cos\theta}\frac{(\alpha+0.5)^2}{\alpha}\overline{D} = 9.35\overline{b}_0^{1/3} + 0.56\overline{b}_0^{2/3} + 2\sqrt{3}\ \frac{R_f}{\sigma_0 t} \tag{20}$$

By substituting $R_f = 3$ N/mm, $\sigma_0 = 110$ MPa, $\theta = \frac{\pi}{4}$ and $\overline{b}_0 = 50$ into Eq. (20), and expanding the left side of Eq. (20) with first-order Taylor series, the following expression can be obtained

$$6.24 + 3.048(\overline{D}) + \mathbf{O}(\overline{D}-1)^2 = 42.05 + \frac{0.06\ (\text{mm})}{t} \tag{21}$$

The final approximation is:

$$\overline{D} = \frac{D}{t} \approx 12.75 + \frac{0.06(\text{mm})}{t} \tag{22}$$

For films with thickness $t \gg 0.06$ mm, the second term in Eq. (22) can be neglected, so the critical $(D/t)_{cr}$ corresponding to the onset of the failure mode transition is equal to 12.75. However, for the films with thickness $t \ll 0.06$ mm, the second term in Eq. (22) cannot be neglected because of its larger value, so $(D/t)_{cr}$ is >12.75. For instance, we use the films with thicknesses of 0.01 mm and 0.025 mm in our experiment, which correspond to 18.75 and 15.15 for $(D/t)_{cr}$, respectively. This observation is consistent with the experimental results shown in Fig. 6, for which the critical transition for D/t is around 15.0.

3.4. Discussion of the effect of the fracture energy

In this work, the fracture energy is considered in both the curling flap and branched concertina tearing models, as shown in Eqs. (2), (6), and (17). We further analyze the effect of the fracture energy on the film cutting force. By using Eqs. (6) and (17), we calculate the energy partition during the cut. When the tool is sharp ($D/t < (D/t)_{cr}$), the curling flap mode occurs. In this situation, Fig. 9a shows the relationship between the energy ratio $(E_{fracture}/E_{total})_{curl}$ and the dimensionless film thickness (Et/R_f), where $E_{fracture}$ and E_{total} are the fracture energy and the total energy (sum of film bending energy and membrane energy), respectively. However, when the tool is blunt ($D/t > (D/t)_{cr}$), the branched concertina mode occurs. In this situation, Fig. 9b shows the relationship between $(E_{fracture}/E_{total})_{concertina}$ and Et/R_f.

Fig. 9 shows that the ratio D/t has a different effect on the two fracture modes. The ratio D/t plays an important role in the curling flap mode, where the energy ratio $(E_{fracture}/E_{total})_{curl}$ decreases as D/t increases, as shown in Fig. 9a. In contrast, as shown in Fig. 9b, the ratio D/t has little effect on $(E_{fracture}/E_{total})_{concertina}$ for the failure of the branched concertina tear. Moreover, we observe that the effect of the fracture energy on the cutting force gradually decreases with the increase of the film thickness. When $Et/R_f > 20000$, the contribution of the fracture energy to the total energy is less than 0.33% for the branched concertina model (Fig. 9b) and less than 1.2% for the curling flap model (Fig. 9a). This fact is consistent with the previous studies for thick plates, which have not considered the fracture energy during the cutting of thick plates (Zheng and Wierzbicki, 1996).

4. Conclusion

In conclusion, experiments and numerical simulations are carried out to study the size effect of tools on the cutting of thin aluminum films. The results show that the failure modes of the cut films are dependent on the tool size: films cut with large tools (large D/t) fail in the form of branched concertina tears, while films cut with small tools (small D/t) fail in the form of curling flaps. The major conclusions are as follows:

(1) We develop a theoretical model (Eq. (6) and Eq. (17)) to predict the cutting force of the two failure modes. For the aluminum film in this study, the critical tool size for the transition of two modes has a value of approximately 15 times the film thickness. This transition is verified by cutting aluminum films with thicknesses in the range of 10 μm to 25 μm.
(2) The two modes have different geometrical features. In the curling flap mode, the wavelength of the curling flap can be determined from Eq. (9). In the branched concertina mode, the length of the tongue L_{tongue} is proportional to the tool diameter D with a coefficient of approximately 2.02.
(3) The contribution of fracture energy to total energy increases with decreasing film thickness. The dependence of $E_{fracture}/E_{total}$ on thickness is insensitive to tool size for the branched concertina mode, but this dependence is very sensitive to tool size for the curling flap mode. As a result, the effect of fracture energy cannot be neglected for aluminum films with micrometer-level thicknesses.

Declaration of Competing Interest

The authors declare that they have no known competing financial interests or personal relationships that could have appeared to influence the work reported in this paper.

Acknowledgments

This work was supported by the National Natural Science Foundation of China (nos. 11902311, 11972347, 11890681, 12022210, 12032001), by the Youth Innovation Promotion Association CAS (no. 2018022), and by the Strategic Priority Research Program of the Chinese Academy of Sciences (no. XDB22040501).

Appendix A

Experimental setup. The dimensions of the aluminum film (length × width × thickness) are 100 mm × 40 mm×(0.01–0.025) mm. Prior to the cutting experiments, two long edges of the film are firmly clamped to a rigid frame with double-sided tape (3 M, USA), while the two short edges are left free (Fig. A1). In addition, an initial 5-mm-long crack is prefabricated in the centerline of one short edge, along which the film is laterally cut with a cylindrical tool driven by a macroscopic material testing system (MTS) (Instron 5942, Instron, USA) in an atmospheric environment, a microscopic MTS (Microtest 200, Gatan, USA) with an optical microscope (HIScope KH-3000, Hirox, Japan), and with scanning electron microscopy (SEM) (SU1510, Hitachi, Japan). The velocity is set to 1 mm/s and the diameter of the cutting tool is controlled in the range of t–500 t. During the cutting experiments, the load–displacement curves are recorded with the MTSs, and the crack propagation process is recorded with a camera. After the experiments, the fracture morphology of the films is observed with SEM.

Simulation details. The cutting of the ultrathin film is simulated using Abaqus/Explicit FEM, for which we use a phase field model with damage (Wang et al., 2020; Wang et al., 2020) to model the thin film. The film is meshed with the four-node quadrilateral shell element with reduced integration (S4R), and the cutting tool is meshed with the eight-node linear solid element with reduced integration (C3D8R). The loading has a smoothed amplitude to mimic the quasi-static process. The mesh size is 0.1 μm in the cracked region of the film where large deformations and damages (cracks) may occur, and the mesh size is 0.5 μm away from the cracked region. We have checked the mesh sensitivity and the results are found to be robust. The materials of the film and the cutting tool are aluminum and steel, respectively, which are for the isotropic elastic–plastic material model. The aluminum film has an elastic modulus of 70 GPa, a yield strength of 110 MPa, and a plastic linear hardening modulus of 1.93 GPa. The steel tool

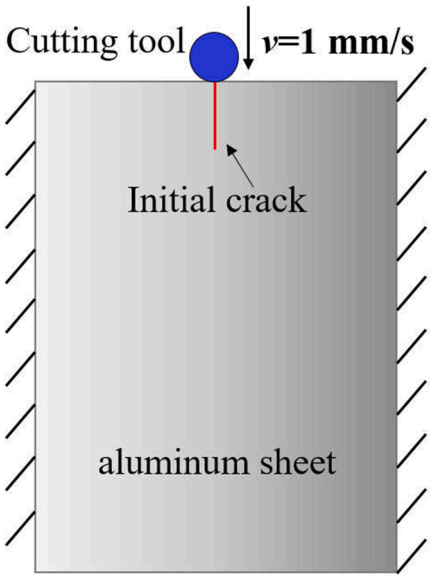

Fig. A1. Schematic diagram of the front view of the cut film experiment. Two long edges of the film are clamped, while the two short edges are left free.

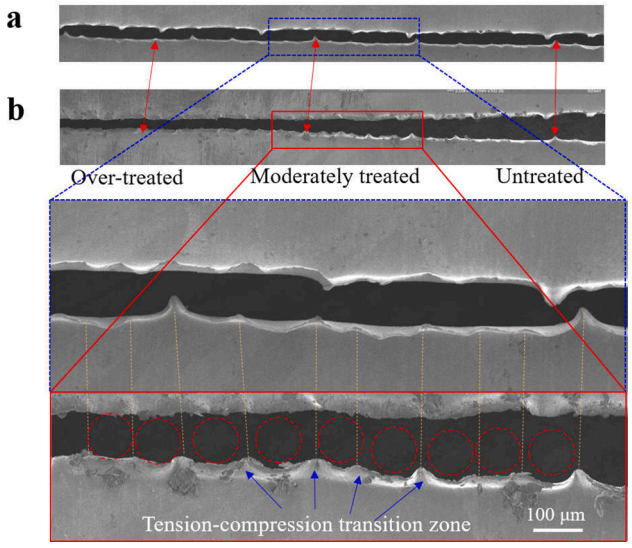

Fig. A4. (a) Morphology of the original curling flap formed after cutting the film with a sharp cylindrical tool and (b) morphology after smoothing treatment.

has an elastic modulus of 162.67 GPa, a yield strength of 247.26 MPa, and a plastic linear hardening modulus of 1.93 GPa (Ye et al., 2020). The fracture energy is determined by trouser-tests (Audoly et al., 2005), and the obtained value is 3 N/mm. The failure process of the aluminum film is simulated using the Abaqus built-in ductile damage model with an initial failure strain of 0.2 and a critical fracture energy of 3 N/mm. In the model, a general contact definition is used for the contact interaction between the film and the cutting tool. The model uses the contact property of a normal hard and tangential friction coefficient of 0.2 for all interactions.

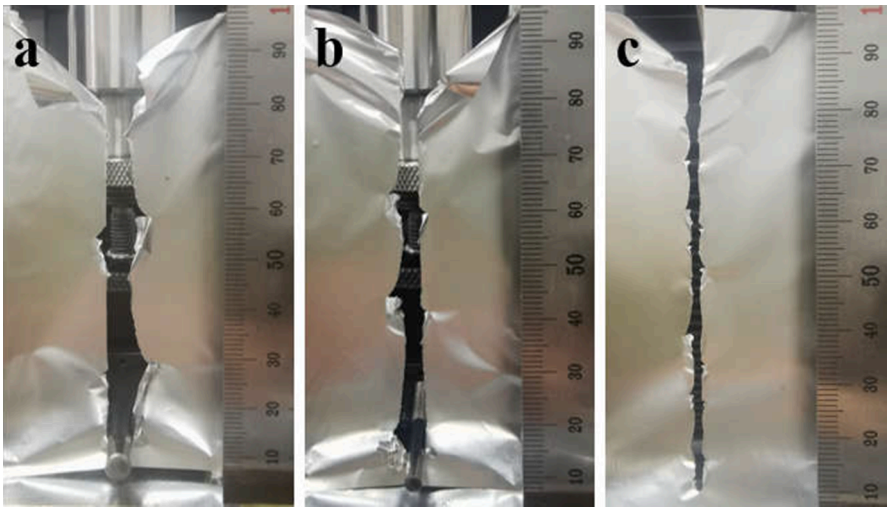

Fig. A2. Experimental results for cylindrical tools with different diameters. (a) $D = 5.22$ mm. (b) $D = 3.43$ mm. (c) $D = 1.35$ mm.

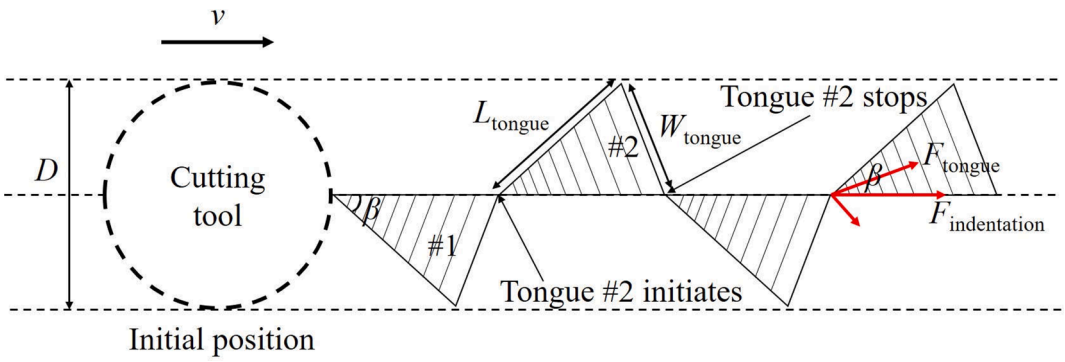

Fig. A3. Configurations of the tongue during the cut.

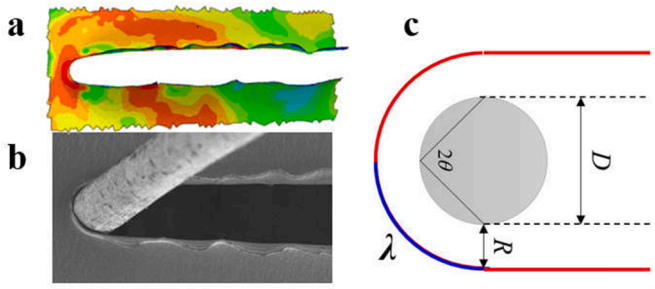

Fig. A5. (a) FEM and (b) experimental results for cutting the film with a sharp cylindrical tool, and (c) schematic diagram of the model, where the blue line represents the wavelength of the periodic curling flap.

Appendix B

The rates of the energy dissipation for bending $\dot{E}_{bending}$ and membrane $\dot{E}_{membrane}$ can be expressed as (Zheng and Wierzbicki, 1996; Magliaro and Altenhof, 2020)

$$\dot{E}_{bending} = 2M_0 v\left(1+\frac{B}{R}\right)$$

$$\dot{E}_{membrane} = \dot{E}_{membrane1} + \dot{E}_{membrane2}$$

$$\dot{E}_{membrane1} = 1.268M_0 v\frac{R}{t}cos\theta$$

$$\dot{E}_{membrane2} = 1.28M_0 v\theta^2\frac{(R+B)^2}{Rt}\frac{cos\left(\frac{\theta}{2}\right)}{cos\theta} \tag{B.1}$$

where $\dot{E}_{membrane1}$ and $\dot{E}_{membrane2}$ are the rates of the membrane energies in the near-tip zone and the tension–compression transition zone, respectively. B and θ are the semi-width and the semi-angle of the wedge, respectively. R is the unknown rolling radius, and M_0 is the fully plastic bending moment.

References

Park, J.S., Maeng, W.-J., Kim, H.-S., Park, J.-S., 2012. Review of recent developments in amorphous oxide semiconductor thin-film transistor devices. Thin Solid Films 520 (6), 1679–1693.

Nie, Z., Kumacheva, E., 2008. Patterning surfaces with functional polymers. Nat. Mater. 7, 277–290.

Yokota, T., et al., 2015. Ultraflexible, large-area, physiological temperature sensors for multipoint measurements. Proc. Natl. Acad. Sci. 112, 14533–14538.

Zheng, S., Chen, M., Li, Z., Wang, H., 2016. Size-dependent constituent equations of piezoelectric bimorphs. Compos. Struct. 150, 1–7.

Pan, H., et al., 2018. Giant energy density and high efficiency achieved in bismuth ferrite-based film capacitors via domain engineering. Nat. Commun. 9, 1813.

Li, H., et al., 2019. Ultrastretchable and superior healable supercapacitors based on a double cross-linked hydrogel electrolyte. Nat. Commun. 10, 536.

Su, Q., Liu, J., Wang, L., Shi, W., Xia, Y., 2006. Efficient CVD diamond film/alumina composite substrate for high density electronic packaging application. Diam. Relat. Mater. 15, 1550–1554.

van den Broek, L.A.M., Knoop, R.J.I., Kappen, F.H.J., Boeriu, C.G., 2015. Chitosan films and blends for packaging material. Carbohydr. Polym. 116, 237–242.

Cazón, P., Velazquez, G., Ramírez, J.A., Vázquez, M., 2017. Polysaccharide-based films and coatings for food packaging: A review. Food Hydrocoll. 68, 136–148.

Hamm, E., Sivak, I., Roman, B., 2020. Nature of crack path instabilities in thin sheets cut by blunt objects. Phys. Rev. Lett. 124, 174101.

Ghatak, A., Mahadevan, L., 2003. Crack street: The cycloidal wake of a cylinder tearing through a thin sheet. Phys. Rev. Lett. 91, 215507.

Audoly, B., Reis, P.M., Roman, B., 2005. Cracks in thin sheets: when geometry rules the fracture path. Phys. Rev. Lett. 95, 025502.

Roman, B., 2013. Fracture path in brittle thin sheets: a unifying review on tearing. Int. J. Fract. 182 (2), 209–237.

Roman, B., Reis, P.M., Audoly, B., De Villiers, S., Viguié, V., Vallet, D., 2003. Oscillatory fracture paths in thin elastic sheets. Comptes Rendus Mécanique 331 (12), 811–816.

Reis, P.M., Kumar, A., Shattuck, M.D., Roman, B., 2008. Unzip instabilities: Straight to oscillatory transitions in the cutting of thin polymer sheets. EPL Europhys. Lett. 82, 64002.

Zheng, Z.M., Wierzbicki, T., 1996. A theoretical study of steady-state wedge cutting through metal plates. Int. J. Fract. 78, 45–66.

Wierzbicki, T., 1995. Concertina tearing of metal plates. Int. J. Solids Struct. 32 (19), 2923–2943.

Wierzbicki, T., Trauth, K.A., Atkins, A.G., 1998. On diverging concertina tearing. J. Appl. Mech. 65, 990–997.

Jin, S.Y., Altenhof, W., 2011. An analytical model on the steady-state deformation of circular tubes under an axial cutting deformation mode. Int. J. Solids Struct. 48, 269–279.

Vandenberghe, N., Villermaux, E., 2013. Geometry and fragmentation of soft brittle impacted bodies. Soft Matter 9 (34), 8162. https://doi.org/10.1039/c3sm50789k.

Abramowicz, W., Jones, N., 1984. Dynamic axial crushing of circular tubes. Int. J. Impact Eng. 2 (3), 263–281.

Guillow, S.R., Lu, G., Grzebieta, R.H., 2001. Quasi-static axial compression of thin-walled circular aluminium tubes. Int. J. Mech. Sci. 43, 2103–2123.

Linul, E., Khezrzadeh, O., 2021. Axial crashworthiness performance of foam-based composite structures under extreme temperature conditions. Compos. Struct. 271, 114156.

Magliaro, J., Altenhof, W., 2020. Mechanical performance and crashworthiness of plates and extrusions subjected to cutting: An overview. Thin-Walled Struct. 148, 106612.

Simonsen, B.C., Wierzbicki, T., 1997. Plasticity, fracture and friction in steady state plate cutting. Int. J. Impact Eng. 19, 667–691.

Lu, G., Calladine, C.R., 1990. On the cutting of a plate by a wedge. Int. J. Mech. Sci. 32, 293–313.

Wierzbicki, T., Thomas, P., 1993. Closed-form solution for wedge cutting force through thin metal sheets. Int. J. Mech. Sci. 35, 209–229.

Paik, J.K., 1994. Cutting of a longitudinally stiffened plate by a wedge. J. Ship Res. 38, 340–348.

Ohtsubo, H., Wang, G., 1995. An upper-bound solution to the problem of plate tearing. J. Mar. Sci. Technol. 1, 46–51.

Jones, N., Jouri, W.S., 1987. A study of plate tearing for ship collision and grounding damage. J. Ship Res. 31, 253–268.
Vaughan, H., 1980. The tearing strength of mild steel plate. J. Ship Res. 24, 96–100.
Woisin, G., 1982. Comments on Vaughan: "The tearing strength of mild steel plate". J. Ship Res. 26, 50–52.
Audoly, B., Pomeau, Y., 2010. Elasticity and geometry: From hair curls to the non-linear response of shells. Oxford University Press.
Tallinen, T., Mahadevan, L., 2011. Forced tearing of ductile and brittle thin sheets. Phys. Rev. Lett. 107, 245502.
Wang, T., Ye, X., Liu, Z., et al., 2020. A phase-field model of thermo-elastic coupled brittle fracture with explicit time integration. Comput. Mech 65, 1305–1321.
Wang, T., Liu, Z., Cui, Y., et al., 2020. A thermo-elastic-plastic phase-field model for simulating the evolution and transition of adiabatic shear band. Part I. Theory and model calibration. Eng. Fract. Mech. 232, 107028.
Ye, X., Hu, J., Song, J., Liu, X., Wei, Y., 2020. Semi-analytical model of the vertical impact of a 316 stainless steel rod. Int. J. Impact Eng. 146, 103694.
Vaughan, H., 1978. Bending and tearing of plate with application to ship bottom damage. Nav. Archit. 3, 97–99.